Journal of Applied Polymer Science

Numerical Simulation on Residual Wall Thickness of Tubes with Dimensional Transitions and Curved Sections in Water-Assisted Injection Molding

Jian-Gen Yang,[1,2] Xiong-Hui Zhou[1]

[1]Institute of Forming Technology & Equipment, National Die and Mold CAD Engineering Research Center, Shanghai Jiaotong University, Shanghai 200030, China

[2]Mechanical and Electronic Engineering Department, Jingdezhen Ceramic Institute, Jingdezhen 333403, China

Correspondence to: X.-H. Zhou (E-mail: xhzhou@sjtu.edu.cn)

ABSTRACT: Residual wall thickness is an important indicator which aims at measuring the quality of water-assisted injection molding (WAIM) parts. The changes of residual wall thickness around dimensional transitions and curved sections are particularly significant. Free interface of the water/melt two-phase was tracked by volume of fluid (VOF) method. Computational fluid dynamics (CFD) method was used to simulate the residual wall thickness, and the results corresponded with that of experiments. The results showed that the penetration of water at the long straight sections was steady, and the distribution of the residual wall thickness was uniform. However, there was melt accumulation phenomenon at the dimensional transitions, and the distribution of the residual wall thickness wasn't uniform. Adding fillet at the dimensional transitions could improve the uniformity of the residual wall thickness distribution, and effectively reduce water fingering. Additionally, at the curved sections, the residual wall thickness of the outer wall was always greater than that of the inner wall, and the fluctuations of the residual wall thickness difference were small. © 2012 Wiley Periodicals, Inc. J. Appl. Polym. Sci. 000: 000–000, 2012

KEYWORDS: molding; theory and modeling; rheology

Received 3 May 2012; accepted 23 July 2012; published online
DOI: 10.1002/app.38394

INTRODUCTION

As a new medium-assisted molding technology, WAIM[1] is the newest way to mold hollow or partly hollow parts. The principle of WAIM is similar to that of gas-assisted injection molding (GAIM),[2] except that the water is incompressible, the viscosity is higher, the thermal conductivity is 40 times, and the heat capacity of which is four times compared to what the nitrogen is. Because of this reason, there are many unique advantages in WAIM: fast cooling, short cycle; thin wall thickness, material savings, lower costs; no sink marks, smooth inner surface. Currently WAIM technology is mainly used in the automotive industry, household items, furniture and building materials which brings a bright future on market prospects.[3]

Residual wall thickness significantly affects the strength of molded parts; so many researchers have investigated the size and distribution of the residual wall thickness by experiments, and achieved lots of research findings.[4–8] On the other hand, the majority of current researches are mainly focused on experiments, while few scholars explain and verify experiments by numerical simulation methods. Li et al.[9] studied the residual wall thickness of tubes through computer simulations, based on the mathematical model of WAIM. Zhang et al.[10] put forward the model and numerical simulation method for the second penetration in WAIM. Khor et al.[11] proved that FLUENT was excellent in handling injection mold filling problems through three-dimensional numerical investigations. In particular, the residual wall thickness around dimensional transitions and curved sections is an important factor in judging the quality of tubes. However, it has never been systematically investigated by numerical simulations.

Reynolds stress was introduced in WAIM model for the turbulence characteristics of high-pressure water, and the traditional injection molding model was improved. Based on the improved mathematical model, the free interface of the water/melt was tracked by VOF method, and CFD method was used to simulate the residual wall thickness. This article mainly studied as the following: (1) the distribution of residual wall thickness at long straight sections; (2) the distribution of residual wall thickness at dimensional transitions and mechanism; (3) the effects of adding fillet to the residual wall thickness distribution; (4) the distribution of residual wall thickness at curved sections. Meanwhile, the simulation results were compared with experimental

data, and it showed that the simulations were reliable. The systematic study of the residual wall thickness at dimensional transitions and curved sections by numerical simulations is greatly needed to enhance the technology of WAIM parts.

MODEL AND METHODS

Mathematical Model

Numerical simulations of the traditional injection molding are based on generalized Hele–Shaw model, which is confined to the thin-walled cavity and used in laminar flow. Whereas, in WAIM, the injection of water is turbulence, and the heat exchange between the water and melt can not be ignored. Therefore, it is necessary to improve the mathematical model.

The filling process in WAIM includes the non-Newtonian laminar of the melt with low Reynolds number and the turbulence of the water injection with high Reynolds number, namely multi-phase stratified unsteady flow. During water assisted filling, the water is injected and penetrates into the core of the melt along the path of the least resistance.

To simplify the flow process and facilitate the simulation, the assumptions are as follows: the water and melt are incompressible; the melt flow meets no-slip boundary, and the melt front is atmospheric pressure; the body forces and surface tension are ignored; the melt fills mold cavity uniformly at the initial state, and the melt injection process doesn't affect water penetration.

Governing equations include the continuity equation, motion equation, energy equation, constitutive equation, viscosity model, and volume fraction equation.

Continuity equation meets the law of mass conservation, and the general form is:

$$\frac{\partial \rho}{\partial t}+\frac{\partial(\rho u_i)}{\partial x_i}=0 \tag{1}$$

The injection of water is high Reynolds number turbulence, so the random nature of turbulent flow must be considered in motion equation. Reynolds stresses are introduced in motion equation based on traditional injection molding, and the Reynolds time-averaged motion equation is:

$$\frac{\partial(\rho u_i)}{\partial t}+\frac{\partial(\rho u_i u_j)}{\partial x_j}=-\frac{\partial p}{\partial x_i}+\frac{\partial}{\partial x_j}\left(\mu\frac{\partial u_i}{\partial x_j}\right)-\frac{\partial}{\partial x_j}(\rho\overline{u_i' u_j'}) \tag{2}$$

where the last item is Reynolds stress.

To deal with Reynolds stress and make the equations close, based on the Boussinesq eddy viscosity assumption, the relationship between Reynolds stress and average velocity gradient is:

$$-\rho\overline{u_i' u_j'}=\mu_t\left(\frac{\partial u_i}{\partial x_j}+\frac{\partial u_j}{\partial x_i}\right)-\frac{2}{3}\left(\rho\kappa+\mu\frac{\partial u_i}{\partial x_j}\right)\delta_{ij} \tag{3}$$

where μ_t denotes turbulent viscosity, and κ denotes turbulent kinetic energy.

Simulated by standard k–ε two-equation turbulence model, the turbulent viscosity equation is:

$$\mu_t=\rho C_\mu\frac{\kappa^2}{\varepsilon} \tag{4}$$

where C_μ denotes empirical constant, and ε denotes dissipation rate.

κ and ε are two basic unknown variables in the standard model, and the delivery equation solving κ and ε is:

$$\frac{\partial(\rho\kappa)}{\partial t}+\frac{\partial(\rho\kappa u_i)}{\partial x_i}=\frac{\partial}{\partial x_j}\left[\left(\mu+\frac{\mu_t}{\sigma_\kappa}\right)\frac{\partial\kappa}{\partial x_j}\right]+G_\kappa-\rho\varepsilon \tag{5}$$

$$\frac{\partial(\rho\varepsilon)}{\partial t}+\frac{\partial(\rho\varepsilon u_i)}{\partial x_i}=\frac{\partial}{\partial x_j}\left[\left(\mu+\frac{\mu_t}{\sigma_\varepsilon}\right)\frac{\partial\varepsilon}{\partial x_j}\right]+\frac{C_{1\varepsilon}\varepsilon}{\kappa}G_\kappa-C_{2\varepsilon}\rho\frac{\varepsilon^2}{\kappa} \tag{6}$$

where $C_{1\varepsilon}$ and $C_{2\varepsilon}$ denote empirical constants, and G_κ denotes the production term of turbulent kinetic energy which is caused by the average velocity gradient.

The heat exchange between the water and melt is considered in the process of injection, and the energy equation is:

$$\frac{\partial(\rho E)}{\partial t}+\frac{\partial}{\partial x_i}[u_i(\rho E+p)]=\frac{\partial}{\partial x_i}\left[\lambda_{\text{eff}}\frac{\partial T}{\partial x_i}+u_i(\tau_{ij})_{\text{eff}}\right] \tag{7}$$

Where E denotes fluid total energy, p denotes melt pressure, λ_{eff} denotes effective thermal conductivity coefficient, and $(\tau_{ij})_{\text{eff}}$ denotes deviatory stress tensor.

The elastic behavior of melt is ignored, and the constitutive equation is:

$$(\tau_{ij})_{\text{eff}}=\eta(p,T,\dot\gamma)\,\dot\gamma \tag{8}$$

Water cools the inside of the melt directly, and the melt temperature in WAIM is lower than that of the other molding. Therefore, Cross-WLF viscosity model is used in simulations. It is a seven-parameter modified model, which can be characterized as the viscosity of the low temperature melt and is closer to the real viscosity of WAIM. The expression of WLF is:

$$\eta(\dot\gamma,T,p)=\frac{\eta_0(T,p)}{1+(\eta_0\dot\gamma/\tau^*)^{1-n}} \tag{9}$$

$$\eta_0(T,p)=D_1\exp\left(-\frac{A_1(T-T^*)}{A_2+(T-T^*)}\right) \tag{10}$$

$$T^*(P)=D_2+D_3p \tag{11}$$

$$A_2=\bar A_2+D_3p \tag{12}$$

where $\eta_0(T,p)$ denotes zero shear viscosity; τ^* denotes material constant, which describes shear stress level transited from Newton viscosity to power-law viscosity; n denotes non-Newtonian index; D_1, D_2, D_3, A_1, and $\bar A_2$ are all material constants.

To make a comparison of the water penetration behavior and residual wall thickness of simulations and literatures,[12–17] polypropylene (PP) is taken as a study resin in this article. Cross-WLF viscosity model parameters of PP are shown in Table I, which are obtained form MOLDFLOW material library.

The actual filling in WAIM is a composite flow that combines the free surface flow with discrete flow of mixtures, in which

Table I. The Parameters of Cross-WLF Viscosity Model

n	τ^* (Pa)	D_1 (Pa s^{-1})	D_2 (k)	D_3 (k/Pa)	A_1	$\bar{A}_2$(k)
0.2569	37655.4	1.2875e+16	263.15	0	37.033	51.6

the free surface flow dominates. As it is impossible to simulate both the flow processes simultaneously, the free interface of the water/melt two-phase is tracked by VOF method. The continuity equation to solve the multiphase volume fraction is:

$$\frac{\partial \alpha_i}{\partial t} + u_i \frac{\partial \alpha_i}{\partial x_i} = 0 \tag{13}$$

Where α_i denotes the volume fraction of the ith phase, which ranges between 0 and 1, and the sum of all phases' volume fraction is equal to 1. α_i takes the value of 1 in cells which contains only the i phase, the value 0 which is void of the i phase, and a value between 0 and 1 which is referred as the i phase front.

Molded Parts and Boundary Conditions

The molded tubes with dimensional transitions and curved sections are shown in Figure 1. Figure 1(a) is the one with a uniform diameter of 10 mm throughout the entire tube, which is used to investigate the residual wall thickness at the long straight sections and curved sections; Figure 1(b) is used for the upstream expansion and downstream contraction; Figure 1(c) is used for the upstream contraction and downstream expansion; Figure 1(d) is used for the dimensional transition with fillet. It shows that all tubes are cylindrical water channel with round cross-section. The tubes aren't axisymmetric on the whole, while it is partly axisymmetric at the long straight sections and dimensional transitions.

To solve the mathematical model, boundary conditions must be specified, which are specified as follows.

Inlet boundary condition of the water injection pressure is specified at the inlet, and the inlet temperature is assumed to be uniform and equal to the water injection temperature, that's:

$$p = p_{\text{in}}, \quad T = T_{\text{water}} \tag{14}$$

Pressure is specified at the outlet, and the outlet pressure is atmospheric pressure, that's:

$$p = p_{\text{out}} = 0 \tag{15}$$

The wall meets no-slip boundary condition, and the method of heat exchange is fixed temperature boundary condition, that's:

$$U = 0, \quad q = h_f(T_w - T_f) \tag{16}$$

where U denotes velocity vector, h_f denotes heat transfer coefficient of the melt, T_w denotes surface temperature of the wall, and T_f denotes melt temperature.

The no-slip condition is applied at the solid-melt interface:

$$U = 0 \tag{17}$$

At core of interface, the boundary condition is:

$$u = v = 0 \tag{18}$$

Moreover, Dirichlet boundary condition[7] is applied at the water–melt interface:

$$T = T_{\text{water}} \tag{19}$$

Testing Process

The molding methods of simulations are short shot, which mean first the mold cavity is partly filled with melt, and then the high-pressure water is injected, finally the water push the melt to fill the cavity fully. The molding material is PP, and the values of processing parameters in simulations are shown in Table II.

Considering the round cross-section of the tubes and time consumption synthetically, two-dimensional simulation models are

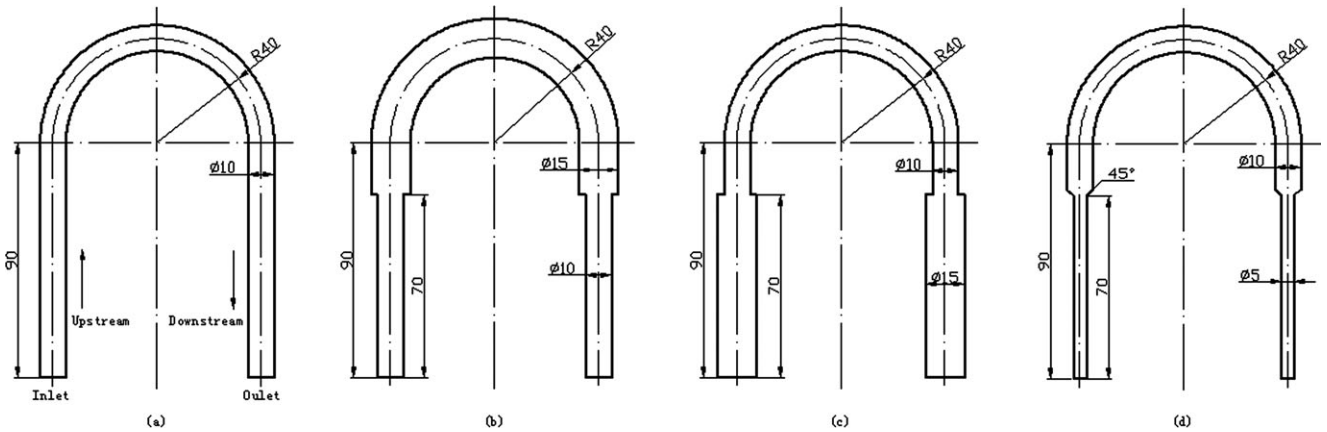

Figure 1. Molded parts with dimensional transitions and curved sections.

Table II. The Processing Parameters in the Simulations

Water pressure (MPa)	Delay time (s)	Melt temp. (K)	Mold temp. (K)	Water temp. (K)	Short shot size (%)
6.5	**0.5**	468	**323**	**313**	**62**
7.5	1	**488**			
8.5	1.5	508			
9.5	2	528			

Bold values are as standard.

built. The calculation domain is discretized with paved mesh of quadrilaterals of 12,840, 16,710, 15,790, and 9368 elements for the four tubes, respectively. Furthermore, the continuity equation, motion equation and energy equation are treated by means of finite volume method, and simultaneously solved by coupling solution.

The solver is 1st-order implicit unsteady formulation. To improve accuracy, the pressure–velocity coupling method adopted is "PISO." In the discretization item settings, the volume fraction is "QUICK," the pressure discrete item is "PRESTO!," and the other items are "First-Order Upwind." For convergence and smoothness of solutions, the under-relaxation factors are all set to 0.3. Besides, unsteady time program is used, with fixed time step size of 10^{-3} s. Computing time per run is 2.4 h on a double processor celeron(R) Duo T3300.

RESULTS AND DISCUSSION

Residual Wall Thickness at Long Straight Sections

Figure 2 is the distribution of residual wall thickness at the long straight sections, which shows that it is uneven nearby the water injection inlet. This is because the water injection velocity is large at the inlet and it's easy to produce turbulent vortex, which results in destabilizing fluctuations at the initial stage of injection molding. At about 1 time cavity diameter away from the inlet, the water begins to penetrate and hollow out the melt at a constant speed. Water penetration remains stable, and the residual wall thickness is uniform. Wu and Liu[12,13] investigated the flow visualization of cavity-filling process in WAIM by experiments, which showed that the penetration of water was quite steady and uniform during the whole filling process, and the water bubble kept almost the same diameter. The water penetration behaviors of simulations are in accord with experimental results.

To demonstrate the size of the molded parts' residual wall thickness comprehensively, hollowed core ratio Φ_h is introduced as a measure index. Φ_h is defined as:

$$\Phi_h = \frac{S_w}{S_p} \times 100\% \quad (20)$$

Figure 2. Residual wall thickness at long straight sections.

where S_w denotes water bubble area, and S_p denotes cross-section area of parts.

Except that the residual wall thickness of the inlet is great, the other sections are thin and uniform, and the hollowed core ratio is from 54 to 61% with the different processing parameters. Liu and Lin[14] studied the residual wall thickness of variable cross-section tubes with the high pressure and flow rate water pin, and the hollowed core ratio obtained changed from 52 to 64%. The simulation result is close to experimental data. Besides, Olley et al.[15] found by simulations and experiments that the hollowed core ratio of parts was from 30 to 56% in GAIM. Compared with that of GAIM, the hollowed core ratio of WAIM is much bigger, so the thinner parts can be made in WAIM. The reason is that the water is incompressible, the viscosity is relatively large, and the rapid cooling of water forms a high viscosity film at the water/melt interface. The film has a larger displacement potential, so that more melt moves along the flow direction, and less melt moves along the wall.

In terms of the effects of processing parameters on the residual wall thickness of the long straight sections, Figure 3 in general shows that the hollowed core ratio increases with the water pressure increasing. This is due to the fact that increasing the water pressure helps the water squeeze the mold wall stronger. It can be seen form Figure 4 that the hollowed core ratio increases as the melt temperature increases. This is because increasing the melt temperature decreases the viscosity of the

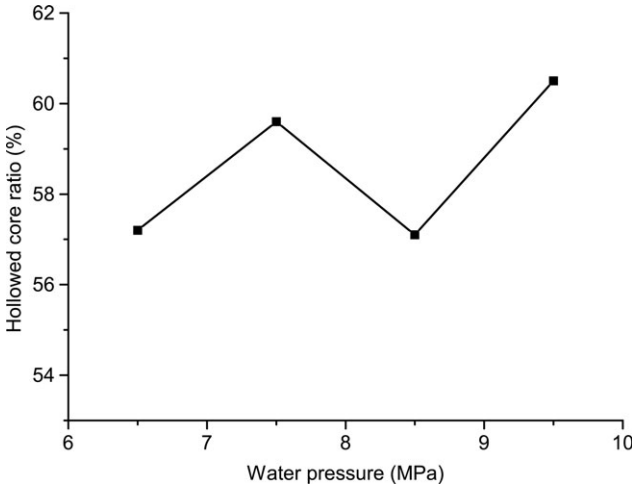

Figure 3. Effect of water pressure on the hollowed core ratios of long straight sections.

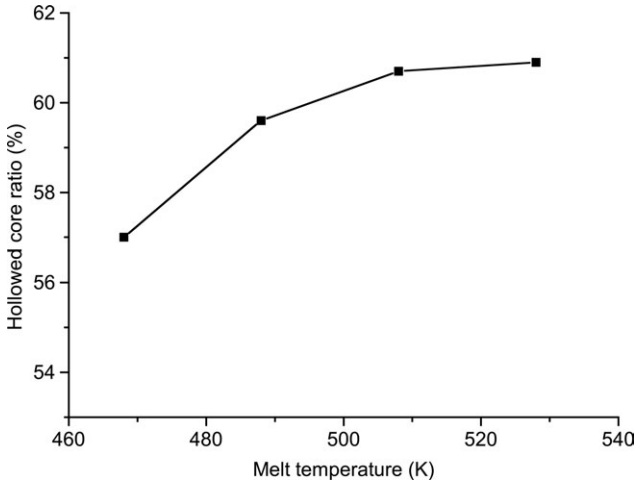

Figure 4. Effect of melt temperature on the hollowed core ratios of long straight sections.

melt, which makes more water penetrate to the mold wall direction. As shown in Figure 5, increasing the delay time leads to the increase of the cooling time and the solidified layer of the melt, and the corresponding decrease in the hollowed core ratio. To sum up, in simulations the effect of the water pressure on the hollowed core ratio agrees well with literatures.[7,14] Besides, the effects of the melt temperature and delay time are also in good agreement with literatures.[4,14]

Residual Wall Thickness at Expansion Transitions

When the water penetrates from the thin area to the thick area, water bubble becomes larger quickly and moves toward the mold wall because of the sudden changes of flow resistance. As the bubble is large enough, it maintains stable and continues to push the melt to flow forward evenly. In the thick area, the velocity of the water and melt is significantly reduced.

Figure 6 shows the distribution of residual wall thickness at upstream expansion transition, where is filled with melt before water penetrates. There is melt accumulation in the corner after

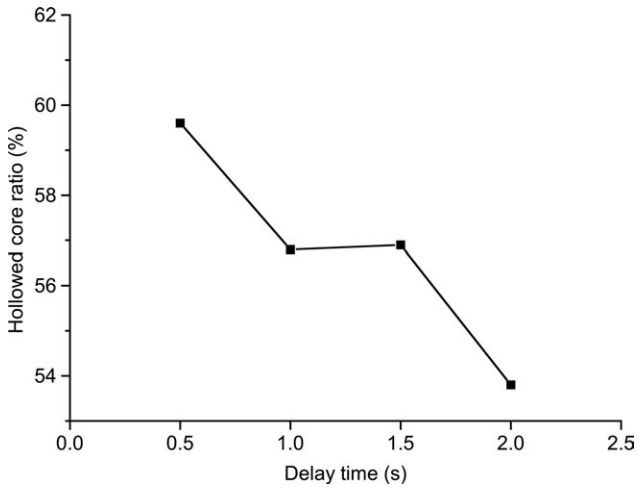

Figure 5. Effect of delay time on the hollowed core ratios of long straight sections.

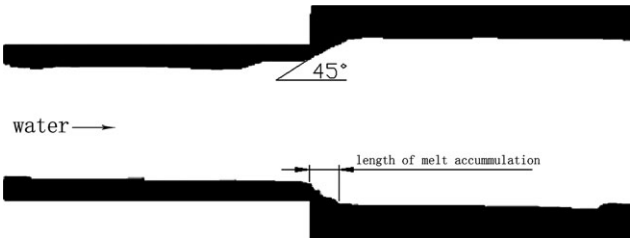

Figure 6. Residual wall thickness at upstream expansion transitions.

water injection, and the boundary of residual wall thickness doesn't resemble the geometry of the mold cavity wall. Rather, a 45-degree edge appears. Figure 7 shows the distribution of residual wall thickness at downstream expansion transition, where isn't filled with melt before water penetrates. The distribution of residual wall thickness after water injection resembles that of upstream expansion transition. Yang and Chou[16] and Liu and Hsieh[17] investigated the distribution of residual wall thickness at upstream and downstream expansion transitions by experiments. The simulation results accord with that of experiments at the upstream expansion transitions. However, at the downstream expansion transitions, the experimental results showed that there was little melt accumulation, the residual wall thickness was uniform, and the boundary of the residual wall resembled the tube geometry. This can be explained as follows. In simulations, the assumptions are that the mold cavity is full of polymer melt at the initial state which has no velocity characteristics, the melt temperature and viscosity distribution are uniform, and the melt injection process does not affect water penetration. Nevertheless, in experiments there is adequate heat transfer for the melt of the water penetration end, and the impacts of the melt injection process can not be ignored.

The water penetration appears "water fingering" phenomenon at the expansion transitions, because of the rapid change of the cross-section dimension. Fingering is that water bubbles penetrate outside designed water channels, enter into the thin area of parts, and form finger-shape branches. The defects seriously affect the performance of parts. To avoid fingering, the structure and dimension of the expansion transitions must be improved. Adding fillet mentioned later is a good way.

The residual wall thickness of the thick area also changes, due to the variation of tubes dimension. Through dimensionless calculation, Kamisli[18] got the analytical expression of residual wall thickness δ:

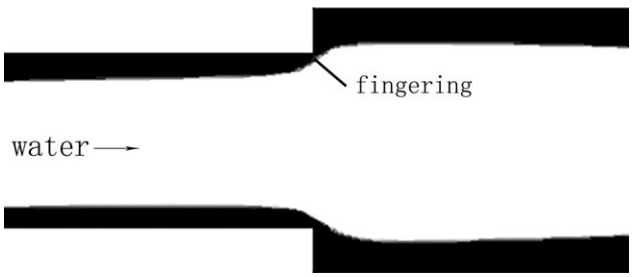

Figure 7. Residual wall thickness at downstream expansion transitions.

Applied Polymer SCIENCE

Figure 8. Residual wall thickness at upstream contraction transitions.

$$\delta = R \cdot b \cdot C_A^{2/3} \tag{21}$$

where b and C_A are defined as follows:

$$b = [2A(\alpha+2)^{2/3\alpha}]^{3\alpha/(\alpha+2)} \tag{22}$$

$$C_A = \eta u_b/\sigma \tag{23}$$

where $\alpha = 1/n$, A depending on α denotes the coefficient of fitting curve, u_b denotes velocity of the water, and σ denotes surface tension.

The residual wall thickness of the thick area becomes bigger, and the hollowed core ratio is 50% which is smaller than 60% of the thin area with the standard processing parameters. It is because that the flow velocity of the melt of the thick area declines, and the weak shearing makes viscosity increase. The impact of viscosity increasing exceeds that of water velocity declining, so that C_A in eq. (23) increases, and δ in eq. (21) also increases.

Furthermore, the rheology of melt significantly affects residual wall thickness, in which there are at least three factors. The first factor is the viscosity of melt. Larger melt viscosity imposes huge resistance for the water flow and makes the water penetration difficult, thus the residual wall thickness will become bigger. The second factor is the non-Newtonian index of melt. Poslinski et al.[19] studied non-Newtonian fluid by experiments and finite element methods and found that the lower non-Newtonian index of melt would get smaller residual wall thickness. Another factor is the shrinkage of melt. During post-filling, high pressure water is injected to compensate the volumetric shrinkage due to the solidifying of melt. The more the melt shrinks, the more the water will penetrate into the melt, or rather, the smaller the residual wall thickness will be.

Residual Wall Thickness at Contraction Transitions

When the water penetrates from the thick area to the thin area, water bubble becomes smaller gradually. As the bubble is small enough, it maintains stable. There has no fingering phenomenon at the contraction transitions which appears at the expansion transitions. It shows that when the water penetrates from the thick area to the thin area, there is no need to take measures to prevent water fingering phenomenon.

Figure 8 shows the distribution of residual wall thickness at upstream contraction transition, where is filled with melt before water penetrates. The boundary of residual wall thickness is smooth, and it doesn't resemble the geometry of the mold cavity wall. Figure 9 shows the distribution of residual wall thickness at downstream contraction transition, where is not filled with melt before water penetrates. The boundary of residual wall thickness is also smooth after water injection. The contraction transitions make the water change in penetration direction and result in convergent streamlines. So, the residual wall thickness at contraction transitions always resembles streamlines, no matter whether it is filled with melt or not when water penetration occurs. Additionally, a comparison of the residual wall thickness of the contraction and expansion transitions displays that the melt accumulation length at the contraction transitions is always greater than that at the expansion transitions. In sum, the model calculation shows good agreement with the experimental results.[17]

Figure 9. Residual wall thickness at downstream contraction transitions.

Residual Wall Thickness at Transition with Fillet

As the water always penetrates along the direction of the least resistance, it is easy to bring water fingering at the expansion transitions. To avoid fingering, the sharp corners of parts must be removed. Liu and Lin[20,21] investigated the factors affecting the formation of fingering, and put forward the measures to reduce the fingering. Learning from these measures, it can be concluded that adding fillet at the expansion transitions will improve fingering effectively. Figure 10 shows the distribution of residual wall thickness at the expansion transition with 45-degree fillet. The water bubble becomes big gradually along the mold boundary, and it continues to penetrate forward after a certain size. The boundary of residual wall thickness is similar to the geometry of the mold cavity wall, and the uniformity of residual wall thickness distribution is greatly improved. The other angle fillets also work well, but it isn't as effective as 45-degree fillet. The shape of the fillet should resemble the inner boundary of the original residual wall at the transition without a fillet for best uniformity.[16,17]

Residual Wall Thickness at Curved Sections

From the above study, we know the distribution of residual wall thickness at the long straight and variable cross-section water

Figure 10. Residual wall thickness with 45° fillet.

channel is axial-symmetrical. Whereas, the residual wall thickness of the inner wall is always thinner than that of the outer wall, and the distribution of residual wall thickness is uneven, as shown in Figure 11. This can be due to the fact that two phenomena occur when the water penetrates into the curved sections: one is the momentum effect. The pressure differences are the same between the water tips and melt tips at all radiuses on condition that the distances decrease with the decrease of the radius. Accordingly, the diving force which is in direct proportion to the pressure difference divided by the distance increases with the decrease of the radius, and the water tends to seek the path of the inner wall. The other is the nonuniform mold wall temperature. At the curved sections, the melt near the inner wall will be a higher temperature due to less steel, which brings a smaller viscosity of the melt near the inner wall. Therefore, the residual wall thickness of the outer wall is greater than that of the inner wall.

The difference of residual wall thickness D is introduced to reflect the distribution uniformity of residual wall thickness of the outer and the inner wall. D is defined as the minus of wall thickness divides the average wall thickness between the outer wall and the inner wall:

$$D = 2(\delta o - \delta i)/(\delta o + \delta i) \quad (24)$$

where δ_o denotes the outer wall thickness, and δ_i denotes the inner wall thickness of parts.

Figure 12 shows the difference of residual wall thickness at five different angles by simulations and experiments,[17] and the results of simulations are consistent with that of experiments. At the 0 degree where is the start point of the curved section, the difference of residual wall thickness is very small, nearly approaching zero. In addition, it changes from 8 to 17% at the other curved angles, and the fluctuations are little. However, in GAIM[17] the fluctuations of the residual wall thickness difference are great, in which the smallest is 7% and the maximum is 52%. Compared with that of GAIM, the difference of residual wall thickness in WAIM is much smaller, so WAIM can get parts with more uniform wall thickness.

CONCLUSIONS

The residual wall thickness of tubes with dimensional transitions and curved sections were simulated by CFD method. In general, the results of simulations corresponded with that of experiments, which verified that CFD was excellent in handling the problems of residual wall thickness in WAIM.

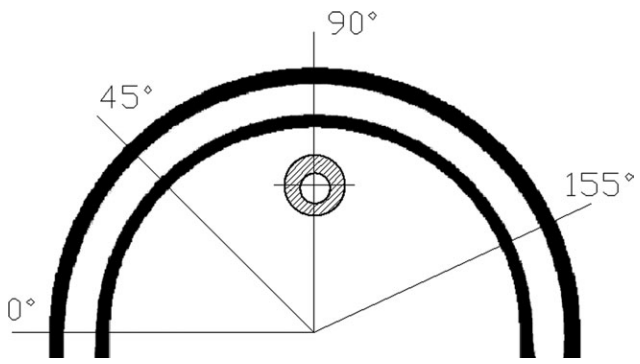

Figure 11. Residual wall thickness at curved sections.

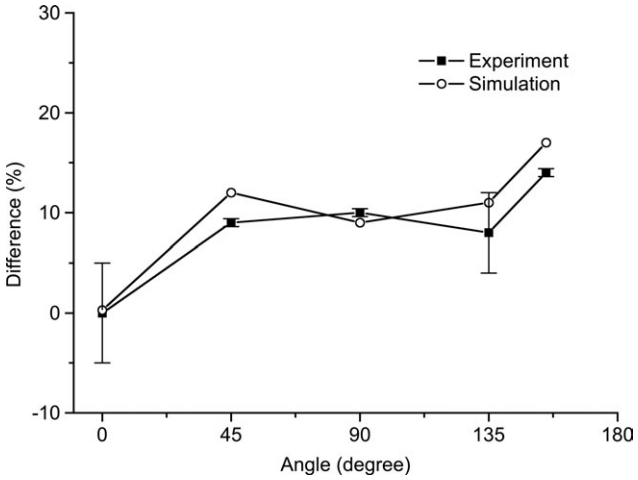

Figure 12. Residual wall thickness difference at curved sections.

At the long straight sections, water penetration remained stable; the distribution of residual wall thickness was uniform. The hollowed core ratio of WAIM was bigger than that of GAIM. Meanwhile, the hollowed core ratio increased with the increases of the water pressure and melt temperature, while it was opposite for the delay time.

There was melt accumulation at the dimensional transitions, and the length of melt accumulation at the contraction transitions was always greater than that of the expansion transitions. Besides, it was easy to occur water fingering at the expansion transitions, while there was no fingering at the contraction transitions. Adding fillet at the dimensional transitions could improve the uniformity of the residual wall thickness distribution, and effectively reduce water fingering.

Furthermore, the residual wall thickness of the outer wall was always greater than that of the inner wall at the curved sections, and the wall thickness difference was inevitable. Compared with that of GAIM, the difference of residual wall thickness in WAIM was smaller, and the parts with more uniform wall thickness could be got.

ACKNOWLEDGMENTS

This work was supported by the Specialized Research Fund (No. 2010B10018) from Science and Technology Bureau of Ningbo City, ZheJiang, China.

REFERENCES

1. Knight, M. *Plast. Tech.* **2002,** *48*, 42.
2. Turng, L. S. *Adv. Polym. Technol.* **1995,** *14*, 1.
3. Protter, R.; Bangerth, H.; Cooper, C. ANTEC Conference Proceedings; Nashville, USA, **2003.**
4. Huang, H. X.; Deng, Z. W. *J. Appl. Polym. Sci.* **2008,** *108*, 228.

5. Wu, Y. C.; Chen, K. M.; Liu, S. *J. Plast. Rubber Compos.* **2006,** *35*, 425.
6. Lin, K. Y.; Chang, F. A.; Liu, S. *J. Int. Commun. Heat Mass.* **2009,** *36*, 491.
7. Polynkin, A.; Bai, L.; Pittman, J. F. T.; Sienz, J.; Mulvaney-Johnson, L.; Brown, E.; Dawson, A.; Coates, P.; Brookshaw, B.; Vinning, K.; Butler, J. *Plast. Rubber Compos.* **2008,** *37*, 131.
8. Ahmad, Z. A.; Amir, H. B. *Polim. W.* **2009,** *54*, 564.
9. Li, Q.; Cao, W.; Zhang, S. X.; Shen, C. Y. *Mater. Sci. Eng.* **2010,** *10*, 1.
10. Zhang, S.; Cao, W.; Zheng, G.; Jia, Z.; Shen, C. *Int. Polym. Proc.* **2011,** *5*, 560.
11. Khor, C. Y.; Ariff, Z. M.; Ani, F. C.; Mujeebu, M. A.; Abdullah, M. K.; Abdullah, M. Z.; Joseph, M. A. *Int. Commun. Heat. Mass.* **2010,** *37*, 131.
12. Wu, Y. C.; Liu, S. *J. Plast. Rubber Compos.* **2005,** *34*, 227.
13. Liu, S. J.; Wu, Y. C. *Polym. Test.* **2006,** *26*, 232.
14. Liu, S. J.; Lin, C. H. *J. Reinf. Plast. Comp.* **2007,** *26*, 1441.
15. Olley, P.; Mulvaney-Johnson, L.; Coates, P. D. *Plast. Rubber Compos.* **2006,** *35*, 47.
16. Yang, S. Y.; Chou, H. L. *Polym. Eng. Sci.* **2002,** *42*, 111.
17. Liu, S. J.; Hsieh, M. H. *Int. Polym. Proc.* **2007,** *22*, 82.
18. Avery, J. Gas-Assist Injection Molding—Principles and Applications; Hanser Gardner Publications: Munich, **2001.**
19. Poslinski, A. J.; Oehler, P. R. Stokes, V. K. *Polym. Eng. Sci.* **1995,** *35*, 877.
20. Liu, S. J.; Lin, S. P. *Compos. A Appl. S.* **2005,** *36*, 1507.
21. Liu, S. J.; Lin, S. P. *Adv. Polym. Tech.* **2006,** *25*, 98.